High-Frequency and -Field Electron Paramagnetic Resonance of High-Spin Manganese(III) in Porphyrinic Complexes

J. Krzystek,*,† Joshua Telser,‡ Luca A. Pardi,†,§ David P. Goldberg,|| Brian M. Hoffman,⊥ and Louis-Claude Brunel†

Center for Interdisciplinary Magnetic Resonance, National High Magnetic Field Laboratory, Florida State University, Tallahassee, Florida 32310, Chemistry Program, Roosevelt University, Chicago, Illinois 60605, Istituto di Fisica Atomica e Molecolare, CNR, 56127 Pisa, Italy, Department of Chemistry, Johns Hopkins University, Baltimore, Maryland 21218, and Department of Chemistry, Northwestern University, Evanston, Illinois 60208

Received February 18, 1999

High-field and -frequency electron paramagnetic resonance (HFEPR) spectroscopy has been used to study two complexes of high-spin manganese(III), d^4, $S = 2$. The complexes studied were (tetraphenylporphyrinato)-manganese(III) chloride and (phthalocyanato)manganese(III) chloride. Our previous HFEPR study (Goldberg, D. P.; Telser, J.; Krzystek, J.; Montalban, A. G.; Brunel, L.-C.; Barrett, A. G. M.; Hoffman, B. M. *J. Am. Chem. Soc.* **1997**, *119*, 8722−8723) included results on the porphyrin complex; however, we were unable to obtain true powder pattern HFEPR spectra, as the crystallites oriented in the intense external magnetic field. In this work we are now able to immobilize the powder, either in an *n*-eicosane mull or KBr pellet and obtain true powder pattern spectra. These spectra have been fully analyzed using spectral simulation software, and a complete set of spin Hamiltonian parameters has been determined for each complex. Both complexes are rigorously axial systems, with relatively low magnitude zero-field splitting: $D \approx -2.3$ cm^{-1} and g values quite close to 2.00. Prior to this work, no experimental nor theoretical data exist for the metal-based electronic energy levels in Mn(III) complexes of porphyrinic ligands. This lack of information is in contrast to other transition metal complexes and is likely due to the dominance of ligand-based transitions in the absorption spectra of Mn(III) complexes of this type. We have therefore made use of theoretical values for the electronic energy levels of (phthalocyanato)copper(II), which electronically resembles these Mn(III) complexes. This analogy works surprisingly well in terms of the agreement between the calculated and experimentally determined EPR parameters. These results show a significant mixing of the triplet ($S = 1$) excited state with the quintet ($S = 2$) ground state in Mn(III) complexes with porphyrinic ligands. This is in agreement with the experimental observation of lower spin ground states in other metalloporphyrinic complexes, such as those of Fe(II) with $S = 1$.

Introduction

The electronic structure of transition metal complexes is of great importance because of the role of these complexes in chemistry and biology. In many cases, the technique of choice to investigate electronic structure is EPR,[1] as many transition metal ions have incompletely filled d shells leading to paramagnetism.[2] In certain paramagnetic transition metal complexes, however, conventional EPR fails to detect resonance transitions. Among such cases are integer spin ($S = 1, 2, \ldots$; "non-Kramers") systems, particularly where the metal ion site has axial symmetry. In these cases, axial zero-field splitting (zfs) removes the zero-field degeneracy of the ground-state spin multiplet yielding a spin ground state that is either a nonmagnetic singlet for positive zfs (i.e., the ground state is $|S, M_S> = |S, 0>$) or a doublet for negative zfs (i.e., since $|S, M_S> = |S, +S>$ and $|S, -S>$ are degenerate in zero field). In the first case (positive zfs), application of a magnetic field has no effect on the $M_S = 0$ ground state. In the second case (negative zfs), the applied field removes the degeneracy of the $M_S = \pm S$ states, but the two are separated by $|\Delta M_S| > 1$, so that a transition between them is "EPR-forbidden". Transitions that involve $M_S = 0 \leftrightarrow \pm 1$, $\pm 1 \leftrightarrow \pm 2$, etc., are "EPR-allowed", but if the zfs is larger than the microwave quantum ($\sim$0.3 cm^{-1} at X-band, 1.2 cm^{-1} at Q-band), then there is either not enough energy to achieve resonance or the resonance would appear at magnetic fields far exceeding those available in standard EPR spectrometers. Such a system would be "EPR-silent"; however, not all integer spin transition metal ion systems are "EPR-silent" at conventional fields and frequencies. If the symmetry is lowered from axial to rhombic, then transitions within the $M_S = \pm 2$ doublet become partially allowed due to state-mixing[2,3] and are EPR-visible, particularly when parallel mode detection is used.[3,4]

† Florida State University.
‡ Roosevelt University.
§ CNR.
|| Johns Hopkins University.
⊥ Northwestern University.

(1) Abbreviations used are as follows: DPDME, deuteroporphyrin IX dimethyl ester; EPR, electron paramagnetic resonance; HFEPR, high-frequency and -field EPR; HS, high spin; LS, low spin; Mn(dbm)$_3$, (1,3-diphenyl-1,3-propanedionato)manganese(III); MnTPPCl, chloro-(5,10,15,20-tetraphenylporphyrinato)manganese(III); MnPcCl, chloro-(phthalocyanato)manganese(III); Pc, dianion of phthalocyanine; py, pyridine; pip, piperdine; TPP, dianion of 5,10,15,20-tetraphenylporphyrin; zfs, zero-field splitting.

(2) Abragam, A.; Bleaney, B. *Electron Paramagnetic Resonance of Transition Ions*; Dover Publications: New York, 1986; pp 399, 434−436, 679.

10.1021/ic9901970 CCC: $18.00
Published on Web 12/10/1999

Many such systems have been successfully investigated by conventional EPR,[3] in particular several comprising monomeric Mn(III).[4−6]

For transition metal systems that are indeed EPR-silent at conventional fields and frequencies, the obvious way to obtain EPR spectra is employ high-frequency and -field EPR (HFEPR).[7−15] This technique has been very successfully applied to high-spin polynuclear transition metal ion clusters[7,16−20] and also to mononuclear Mn(III)[21,22] and Cr(II),[23] both $S = 2$. Our interest in Mn(III) stems from the role of this ion in biological systems, such as superoxide dismutase,[4,24] and in synthetic chemistry, wherein Mn(III) porphyrins[25] and phthalocyanines[26] have been used as building blocks in the construction of molecule-based magnets.

Our previous communication on Mn(III) porphyrinic-type complexes[21] described the first successful detection of allowed HFEPR transitions in an axial HS $3d^4$ system. This experiment was performed on polycrystalline samples which underwent a mechanical torquing effect so effective that almost 100% of the crystallites oriented themselves in such a way that the axis of the largest zfs anisotropy, *z*, was parallel to the applied magnetic field (B_0). Consequently, the resulting spectra were of "quasi-single crystal" quality since only the $B_0 \| z$ transitions could be observed. This effect, observed also in conventional fields, is much more pronounced at the high fields employed in HFEPR. It is particularly manifest in spin systems characterized by a negative zfs parameter *D* which implies that their ground spin state (in the case of HS Mn(III), $|S, M_S> = |2, -2>$) has a magnetic moment. The quasi-single-crystal quality of the spectra obtained for that series of Mn(III) complexes allowed their straightforward interpretation and estimation of the spin Hamiltonian parameters along the *z* principal axis: *D* and $g_{\|}$. To validate this particular analysis on the basis of a restricted set of EPR transitions and in general to understand the *overall* electronic structure of a non-Kramers system by HFEPR, it is necessary to base the interpretation on a true powder pattern spectrum, which includes transitions along all principal axes of the zfs tensor (*x* and *y* as well as *z)*. The principal objective of this work is to obtain such complete powder spectra of the Mn(III) ion and elucidate its electronic structure in two complexes: (tetraphenylporphyrinato)manganese(III) chloride (MnTPPCl) and its closely related analogue (phthalocyanato)manganese(III) chloride (MnPcCl).

Experimental Section

Materials and Samples. MnTPPCl was purchased from Porphyrin Products. The sample had a form of small dark-green needle-shaped crystals discernible by eye. MnPcCl (97% purity) was purchased from Aldrich and used without further processing. Its consistency was of much finer powder than the MnTPPCl. To prevent the effect of torquing in a magnetic field, both samples were carefully ground, and then either (a) immersed in molten *n*-eicosane (Sigma, $C_{20}H_{42}$, mp 37 °C), which was then allowed to solidify forming a hard wax, or (b) mixed with powdered KBr and pressed into a pellet, similarly to the sample preparation method used in infrared spectroscopy. The typical sample amount was 10−20 mg.

HFEPR Experiments. HFEPR spectra were recorded on a spectrometer analogous to that described by Mueller et al.[27] It has been briefly described[15] and will be elaborated on in a forthcoming paper.[28] Its sensitivity is $\leq 10^{13}$ spins/G at $T = 300$ K and $\leq 10^{11}$ spins/G at $T = 10$ K as checked with standards.[28] The spectrometer has fundamental microwave frequencies of 95 ± 3 and 110 ± 3 GHz, from which higher harmonics can be also generated to yield the multiplicities of these frequencies. A set of high-pass filters removes the fundamentals and lower harmonics. Higher harmonics (up to the fifth) on the other hand do get through and care is necessary to identify them in the detected spectra, which is done by running an experiment at the same fundamental frequency and changing the filters in a series from the lowest one (×2) to the highest available (×5). Due to the spread of resonances over the entire field range (15 T) available at the magnet temperature of 4.2 K, relatively rapid field scans were required (0.3−0.5 T/min). This results in a field hysteresis as measured by monitoring the magnet power supply current. The hysteresis was accounted for by sweeping the field in both directions and assuming the resonance field as the average from the two scans. This procedure creates an error of < 5 mT as checked by standards, which is about 1 order of magnitude less than the line width of the signals detected in polycrystalline Mn(III) complexes. The main solenoid linearity was checked by two independent methods (EPR using a field marker DPPH and NMR using proton and deuterium probes) and found to be better than 0.02 mT/A (with the 14.5 T current equal to 116 A) at least in the 3.9−11.8 T range.

HFEPR Analysis. The magnetic properties of an ion with $S = 2$ can be described by the standard spin Hamiltonian comprised of Zeeman and zfs terms:

$$\mathbf{H} = \beta B \mathbf{g} S + D(S_z^2 - S(S+1)/3) + E(S_x^2 - S_y^2) \qquad (1)$$

We employed several methods to apply eq 1 in analyzing the experimental EPR spectra. Analytical solutions exist to calculate the

(3) Münck, E.; Surerus, K. K.; Hendrich, M. P. *Methods Enzymol., Part D* **1993**, *227*, 463−479.
(4) Campbell, K. A.; Yikilmaz, E.; Grant, C. V.; Gregor, W.; Miller, A.-F.; Britt, R. D. *J. Am. Chem. Soc.* **1999**, *121*, 4714−4715.
(5) Dexheimer, S. L.; Gohdes, J. W.; Chan, M. K.; Hagen, K. S.; Armstrong, W. H.; Klein, M. P. *J. Am. Chem. Soc.* **1989**, *111*, 8923−8925.
(6) Gerritsen, H. J.; Sabisky, E. S. *Phys. Rev.* **1963**, *132*, 1507−1512.
(7) Barra, A.-L.; Brunel, L.-C.; Gatteschi, D.; Pardi, L.; Sessoli, R. *Acc. Chem. Res.* **1998**, *31*, 460−466.
(8) Möbius, K. *Appl. Magn. Reson.* **1995**, *9*, 389−407.
(9) Smirnova, T. I.; Smirnov, A. I.; Clarkson, R. B.; Belford, R. L. *J. Phys. Chem.* **1995**, *99*, 9008−9016.
(10) Coremans, J. W. A.; Poluektov, O. G.; Groenen, E. J. J.; Canters, G. W.; Nar, H.; Messerschmidt, A. *J. Am. Chem. Soc.* **1994**, *118*, 12141−12153.
(11) Lebedev, Y. S. *Appl. Magn. Reson.* **1994**, *7*, 339−362.
(12) Lynch, W. B.; Boorse, R. S.; Freed, J. H. *J. Am. Chem. Soc.* **1993**, *115*, 10909−10915.
(13) Brunel, L.-C. *Physica B* **1995**, *211*, 360−362.
(14) Brunel, L.-C.; Barra, A.-L.; Martinez, G. *Physica B* **1995**, *204*, 298−302.
(15) Krzystek, J.; Sienkiewicz, A.; Pardi, L.; Brunel, L.-C. *J. Magn. Reson.* **1997**, *125*, 207−211.
(16) Caneschi, A.; Gatteschi, D.; Sessoli, R.; Barra, A.-L.; Brunel, L.-C.; Guillot, M. *J. Am. Chem. Soc.* **1991**, *113*, 5873−5874.
(17) Barra, A.-L.; Caneschi, A.; Gatteschi, D.; Sessoli, R. *J. Am. Chem. Soc.* **1995**, *117*, 8855−8856.
(18) Delfs, C.; Gatteschi, D.; Pardi, L.; Sessoli, R.; Wieghardt, K.; Hanke, D. *Inorg. Chem.* **1993**, *32*, 3099−3103.
(19) Rentschler, E.; Gatteschi, D.; Cornia, A.; Fabretti, A. C.; Barra, A.-L.; Shchegolikhina, O. I.; Zhdanov, A. A. *Inorg. Chem.* **1996**, *35*, 4427−4431.
(20) Barra, A.-L.; Gatteschi, D.; Sessoli, R. *Phys. Rev. B* **1997**, *56*, 8192−8198.
(21) Goldberg, D. P.; Telser, J.; Krzystek, J.; Montalban, A. G.; Brunel, L.-C.; Barrett, A. G. M.; Hoffman, B. M. *J. Am. Chem. Soc.* **1997**, *119*, 8722−8723.
(22) Barra, A.-L.; Gatteschi, D.; Sessoli, R.; Abbati, G. L.; Cornia, A.; Fabretti, A. C.; Uytterhoeven, M. G. *Angew. Chem., Int. Ed. Engl.* **1997**, *36*, 2329−2331.
(23) Telser, J.; Pardi, L. A.; Krzystek, J.; Brunel, L.-C. *Inorg. Chem.* **1998**, *37*, 5769−5775.
(24) Fridovich, I. *Annu. Rev. Biochem.* **1995,** *64*, 97−112.
(25) Miller, J. S.; Calabrese, J. C.; McLean, R. S.; Epstein, A. J. *Adv. Mater.* **1992**, *4*, 498−501.
(26) Miller, J. S.; Vazquez, C.; Calabrese, J. C.; McLean, R. S.; Epstein, A. J. *Adv. Mater.* **1994,** *6*, 217−221.
(27) Mueller, F.; Hopkins, M. A.; Coron, N.; Grynberg, M.; Brunel, L.-C.; Martinez, G. *Rev. Sci. Instrum.* **1989**, *60*, 3681−3684.
(28) Hassan, A. K.; Pardi, L. A.; Krzystek, J.; Sienkiewicz, A.; Goy, P.; Rohrer, M.; Brunel, L.-C. *J. Magn. Reson.*, in press.

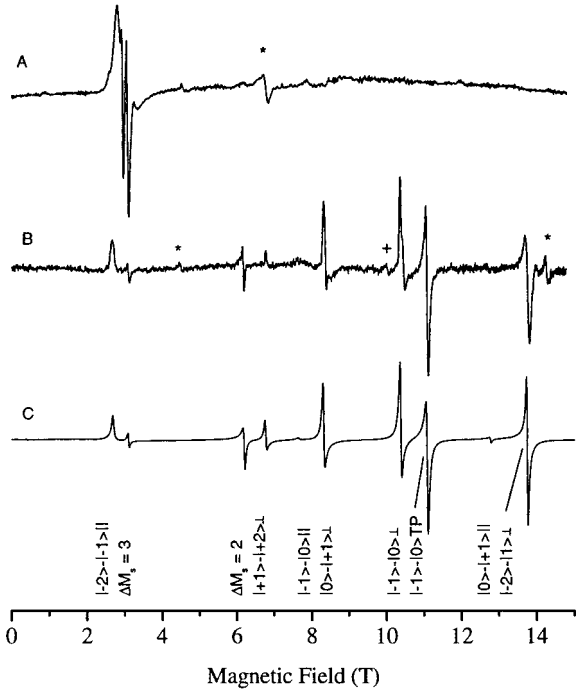

Figure 1. HFEPR spectra of MnTPPCl: (A) polycrystalline sample; (B) sample ground and immobilized with *n*-eicosane; (C) spectrum simulated using parameters as in Table 1. Experimental conditions: frequency, 280.53 GHz; temperature, 5 K (A) and 10 K (B and C); field sweep rate, 0.5 T/min below 12 T and 0.25 T/min above 12 T; field modulation frequency, 8 kHz; modulation amplitude 1.5 mT; time constant, 0.3 s. The particular spin transitions in the simulated spectrum are identified and labeled accordingly. In the simulations, the single-crystal line width was set at 30 mT for the parallel transitions and 35 mT for the perpendicular ones. The transitions marked with an asterisk (∗) in the experimental spectra originate from a higher harmonic of the source (i.e. 374 GHz) while the transition marked with a plus (+) originates from a $g = 2$ Kramers-type impurity; neither are therefore reproduced in the simulations.

energy levels for B_0 parallel or perpendicular to the principal zfs (z) axis of an $S = 2$ system.[29] A computer program was also used to calculate the EPR transition energies and probabilities from the eigenvalues and eigenvectors, respectively, obtained by diagonalization (using the EISPACK subroutines) of the spin Hamiltonian matrix resulting from eq 1, again with B_0 parallel or perpendicular to the z axis. The program source code is available from J. Telser. A program written by Weihe[30] was used to generate powder pattern EPR spectra, allowing direct assignment of the observed EPR transitions. This program was also employed by Barra et al. in their analysis of Mn(dbm)$_3$,[22] as well as in our previous study of aqueous Cr(II),[23] and in numerous $S > {}^1/_2$ Kramers systems.[30]

Results and Discussion

HFEPR Spectra. The low-temperature HFEPR spectrum of a polycrystalline sample of MnTPPCl at ca. 280 GHz is presented in Figure 1A. It consists of one strong peak at about 2.5 T, previously interpreted[21] as having its origin in the parallel $|S, M_S\rangle = |2, -2\rangle \rightarrow |2, -1\rangle$ transition and a superimposed second peak which is identified as a partially allowed ($\Delta M_S = \pm 3$) transition. The absence of other peaks, corresponding to perpendicular orientations of the crystallites with respect to the magnetic field, is due to a very strong torquing effect which aligns almost all crystallites along external field so that the maximum zfs anisotropy axis z is parallel to the field. The spectrum could thus be called "quasi-single crystal" except for the visible structure which was also detected in the previous study and which is an artifact due to the incomplete orientation of the crystallites. The weaker peak at about 6.5 T is the same parallel $|-2\rangle \rightarrow |-1\rangle$ transition induced by harmonic no. 4 of the basic source frequency, i.e., ∼374 GHz. At sufficiently high temperature (20 K) the next parallel transition, i.e., $|-1\rangle \rightarrow |0\rangle$ appears in the spectrum (not shown), but there is essentially no trace of any perpendicular transition discernible at any temperature. None of the observed signals showed any hyperfine structure due to the manganese nuclear spin $I = {}^5/_2$, and it was not expected given that the systems under study were concentrated spin systems undergoing strong line broadening due to spin−spin interactions.

In an attempt to observe also perpendicular transitions in the powder pattern spectra we thus purposefully destroyed the alignment effect by reducing the crystallite size through grinding and prevented orientation by immobilizing the powder. This was accomplished in either of two ways: the sample powder was mixed with molten *n*-eicosane which rapidly froze or the sample was ground with KBr and pressed into a pellet. In the case of MnTPPCl, the former method worked better although the absorption of millimeter and submillimeter radiation by *n*-eicosane caused a decrease in the signal-to-noise ratio. Figure 1B shows a 280 GHz HFEPR spectrum of the same sample as in Figure 1A but subjected to the treatment described above. The spectrum is changed dramatically: there appears a new peak at ca. 13.8 T which now has the largest intensity at low temperature (below 10 K). Upon lowering of the temperature, both $|-2\rangle \rightarrow |-1\rangle$ transitions dominate the spectra since the $|S, M_s\rangle = |2, -2\rangle$ level is the only one significantly populated. With $T > 10$ K the changes are limited to intensities only (and confirming the negative D). At higher T, however, the signal-to-noise ratio decreases; we have therefore restricted ourselves to presenting only spectra taken at 10 K. An immediate qualitative interpretation of the spectrum suggests that this new peak corresponds to the perpendicular orientation of the zfs tensor relative to the magnetic field. This interpretation was confirmed by the simulations (Figure 1C) which identify not only this perpendicular $|-2\rangle \rightarrow |-1\rangle$ transition but also a multitude of other allowed, or partially allowed transitions, as discussed below. We have also performed HFEPR experiments on the same sample at a frequency much lower (109 GHz), and much higher (374 GHz), than that in Figure 1. These experimental spectra are presented in Figure 2, and each of them is accompanied by its simulation. As expected, the 374 GHz spectrum is shifted to higher fields than at 280 GHz, so that the previously observed perpendicular $|-2\rangle \rightarrow |-1\rangle$ transition moves outside the magnet field range (15 T at a magnet temperature 4.2 K). Many additional peaks appear at low fields, however, and these are identified in the Figure 2 and will be discussed below. The spectrum at 109 GHz, although simpler and shifted to lower fields, is not easy to interpret qualitatively but will also be discussed below. The agreement between the simulated and experimentally achieved line shapes convinced us that a truly random distribution of microcrystallites was obtained. We have also tried frozen solution experiments of the two complexes under study but were unable to obtain satisfactory powder patterns.

(29) Baranowski, J.; Cukierda, T.; Jezowska-Trzebiatowska, B.; Kozlowski, H. *J. Magn. Reson.* **1979**, *33*, 585−593. We note that there is an error on p 586; the variable p_1 is incorrectly set equal to b_1 and should be set to B_1. This change is necessary to obtain a correct energy level diagram.

(30) Jacobsen, C. J. H.; Pedersen, E.; Villadsen, J.; Weihe, H. *Inorg. Chem.* **1993**, *32*, 1216−1221. The simulation software package is freely distributed by Dr. H. Weihe; for more information see the following WWW page: http://sophus.kiku.dk/epr/epr.html.

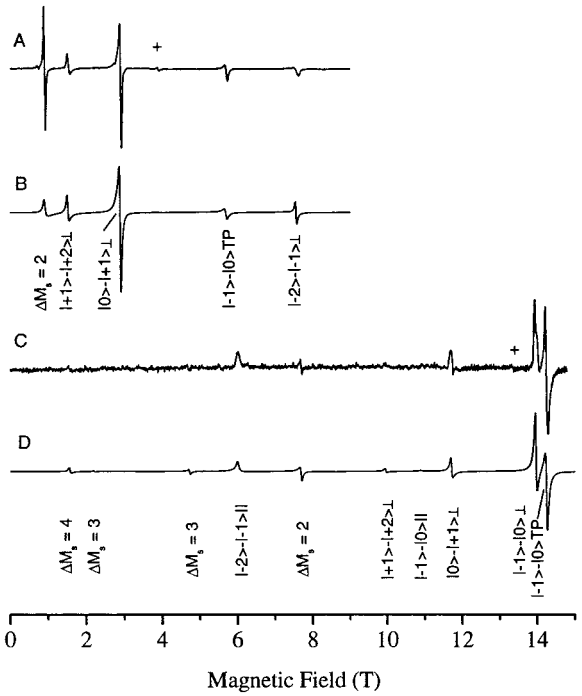

Figure 2. Representative HFEPR spectra of MnTPPCl at low and high frequencies: (A) 108.99 GHz spectrum of a sample ground and immobilized with *n*-eicosane; (B) 108.99 GHz spectrum simulated using parameters as in Table 1; (C) 374.28 GHz spectrum of sample ground and immobilized with eicosane; (D) 374.28 GHz spectrum simulated using parameters as in Table 1. Other experimental conditions are as in Figure 1. The particular spin transitions in the simulated spectrum are identified and labeled accordingly. In the simulations, the single-crystal line width was set at 30 mT for the parallel transitions and 35 mT for the perpendicular ones. The transitions marked with a plus (+) originate from a $g = 2$ Kramers-type impurity and are therefore not reproduced in the simulations.

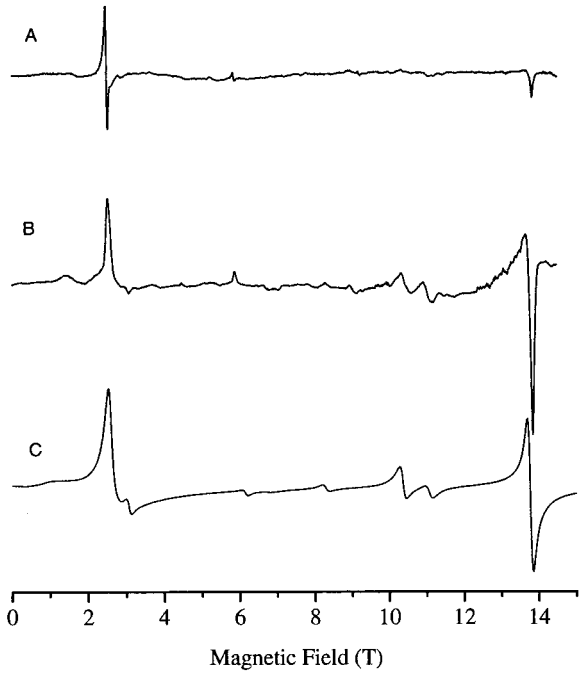

Figure 3. HFEPR spectra of MnPcCl: (A) polycrystalline sample; (B) sample ground with KBr and pressed into a pellet; (C) spectrum simulated using parameters as in Table 1. Experimental conditions: frequency, 279.12 GHz (A) and 280.14 GHz (B and C); temperature, 5 K; other conditions as in Figure 1. In the simulations, the single-crystal line width was set at 80 mT for the parallel transitions and 120 mT for the perpendicular ones.

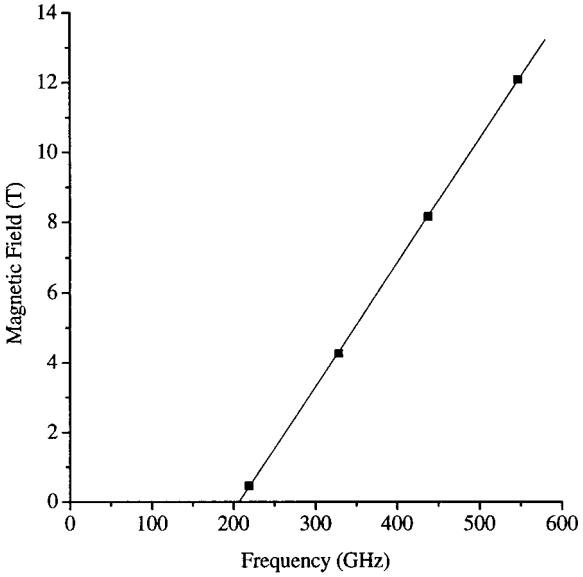

Figure 4. Resonance field vs frequency plot of the parallel $|-2> \rightarrow |-1>$ EPR transition in polycrystalline MnPcCl sample at 5 K. The linear fit yields the following parameters: $D = -2.28$ cm^{-1}; $g = 2.02$.

HFEPR spectra of MnPcCl are shown in Figure 3. In this case, we also recorded a spectrum with the sample "as is", which is shown in Figure 3A. As expected, the spectrum at 280 GHz and 5 K is dominated by the parallel $|-2> \rightarrow |-1>$ line at 2.4 T as in the case of MnTPPCl; however, unlike in MnTPPCl, the perpendicular $|-2> \rightarrow |-1>$ transition is also visible in the spectrum at ca. 13.8 T. The intensities of both signals are reversed in comparison with the expected powder pattern spectra. This means that the MnPcCl crystallites still undergo the torquing effect; however, the torque is smaller than in the case of MnTPPCl and the alignment is only partial. This most certainly results from the much smaller crystallite size for the MnPcCl sample. Treatment with either *n*-eicosane or a KBr pellet changes the spectrum similarly to the MnTPPCl system, as shown in Figure 3B. However, the experimental HFEPR spectra of randomized MnPcCl are not as nice as for MnTPPCl. The spectra show multiple features which do not correspond to any turning points, and while the spectral position of the resonance peaks can be simulated to a good degree (Figure 3C), neither the simulated intensity nor shape is in as good agreement with experiment as in the case of MnTPPCl. The most probable reason is the less than perfectly random distribution of crystallites, despite the immobilization procedures. It should be also noted that, in the case of MnPcCl, the *n*-eicosane method yielded less satisfactory spectra than the KBr pellet procedure. To facilitate the consequent analysis of spin-Hamiltonian parameters for MnPcCl HFEPR we performed a multifrequency study of the sample "as is" analogously to the method applied previously to MnTPPCl.[21] The dominant parallel $|-2> \rightarrow |-1>$ transition was then followed in the 220−550 GHz frequency range. The resulting plot of resonance field versus frequency is shown in Figure 4.

Spectral Interpretation. To analyze the HFEPR spectra of MnTPPCl and MnPcCl, we first plotted the magnetic field dependence of the electronic spin sublevels characterizing the $S = 2$ state[29] with $D = -2.27$ cm^{-1}, $E = 0$, and g (isotropic) $= 2.00$, as established for MnTPPCl in the previous study.[21] We then proceeded to plot the resonance field vs quantum energy dependence of the individual transitions within the $S =$

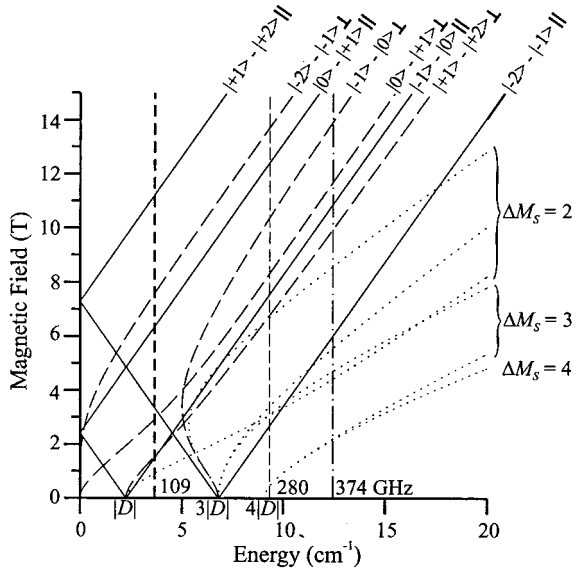

Figure 5. Plot of resonance field vs transition energy for MnTPPCl using spin Hamiltonian with $S = 2$, $D = -2.29$ cm^{-1}, $E = 0$, and $g_{||} = g_{\perp} = 2.00$. The solid lines are the EPR resonance branches for B_0 along z ($B_{||}$), and the dashed line are those for B_0 along x ($B_{\perp}$) both for $\Delta M_S = \pm 1$ (fully allowed); the dotted lines are those for B_z with $|\Delta M_S| > 1$ (partially allowed). The ground state $|M_S>$ to excited state $|M_S>$ levels are indicated, based on a energy level diagram for this system (not shown). The transition energies are calculated by diagonalization of the spin Hamiltonian matrix. The three vertical lines correspond to the frequencies at which data in Figures 1 and 2 were taken.

2 manifold (Figure 5). To facilitate the interpretation of the spectra, we have included three intersects at quantum energies corresponding to 109, 280, and 374 GHz, equal to the frequencies at which spectra in Figures 1 and 2 were taken. One can see from that plot that at 109 GHz, the $|-2> \rightarrow |-1>$ parallel transition which appears in the experimental spectra at higher frequencies, is not detectable. The next parallel transition, $|-1> \rightarrow |0>$, coincides with the perpendicular $|+1> \rightarrow |+2>$ transition and is therefore not detectable either. The other two parallel transitions possible to detect are those originating from the $|+2>$ and $|+1>$ spin sublevels which are not expected to be significantly populated at 10 K. Thus there are no parallel transitions in the 109 GHz spectrum. There are, however, three perpendicular transitions that appear at $\leq$ 2 T, $\sim$3 T, and $\sim$7 T, respectively. These are all visible in Figure 2A. Additionally, there is a partially allowed transition at low field ($\sim$1 T) which also appears in the experimental spectrum. The only remaining peak in the experimental spectrum is at $\sim$6 T, which is not easily interpretable based on the plot in Figure 5; it will be discussed together with the simulation results below.

The intersect at 280 GHz in Figure 5 shows that the first parallel transition from the ground $|-2>$ state appears at just above 2 T, with the next parallel transition $|-1> \rightarrow |-0>$ barely visible at just below 8 T. The perpendicular transitions clearly dominate the spectrum, with the one corresponding to $|-2> \rightarrow |-1>$ showing up just below 14 T. The perpendicular $|-1> \rightarrow |0>$ transition appears doubled between 10 and 11 T for reasons postponed until discussing simulations. Finally, the intersect at 374 GHz explains why the perpendicular $|-2> \rightarrow |-1>$ transition disappears from the magnet field range and the dominant peaks belonging to the "twinned" $|-1> \rightarrow |0>$ transition appear at close to 14 T. The appearance of several peaks at low fields (<4 T) in the experimental spectra is explained by the partially allowed transitions with $\Delta M_S = \pm 2$, ± 3, and ± 4 character.

Table 1. Spin Hamiltonian Parameters of Mn(III) Systems

	D (cm^{-1})	E (cm^{-1})	$g_{||}$[g]	$g_{\perp}$[g]
Porphyrinic Complexes				
MnTPPCl[a]	−2.290(5)	0.00(1)	1.98(2)	2.005(3)
MnPcCl[a]	−2.31(1)	0.00(1)	2.00(2)	2.005(5)
MnTPP(ClO_4)[b]	−2.0		2	2
MnTPP(py)Cl[c]	−3.0(3)		2	2
MnDPDME Cl[d]	−2.53(2)	∼0.01	2	2
MnDPDME Br[d]	−1.1(1)	∼0	2	2
Other Complexes				
$Mn(dbm)_3$[e]	−4.35	0.26	1.97	1.99
$\{Mn^{3+}\}TiO_2$[f]	−3.4(1)	0.116(1)	1.99(1)	2.00(2)

[a] This work; magnetic susceptibility data for MnTPPCl gave $D = -2.3(2)$ cm^{-1}.[32] [b] Magnetic susceptibility data from ref 32. [c] Magnetic susceptibility data from ref 31. [d] DPDME is deuterioporphyrin IX dimethyl ester; far-IR data from ref 33. [e] dbm is 1,3-diphenyl-1,3-propanedione; HFEPR data from ref 22. [f] Mn^{3+} dopant in rutile; EPR data from ref 6. [g] g values were assumed to equal 2 except in EPR studies where they were explicitly determined.

The HFEPR spectra of MnPcCl very closely follow those of MnTPPCl. Their quality however is less spectacular, and many of the weaker transitions that are visible in the MnTPPCl spectra disappear in the features in the MnPcCl spectra which were discussed in the previous subsection.

Simulations. The previous study[21] determined spin Hamiltonian parameters on the basis of resonance field vs frequency dependence of a single peak, corresponding to the parallel $|-2> \rightarrow |-1>$ transition. It is desirable to base a quantitative analysis on multiple transitions rather than a single one, and this was done by means of spectral simulations of the powder pattern spectra obtained in this study. The simulation program is described elsewhere.[30] For our purposes it is sufficient to underscore that it is based on a full-matrix diagonalization procedure and is therefore adequate to spin systems with any value of zfs parameters relative to the operating frequency. It operates in two steps: step 1 calculates the resonance fields and the transition intensities, while step 2 constructs a powder pattern using the anisotropic line width of a single-crystal transition as a parameter. The program assumes a collinearity of the g and zfs tensors, as is usually done in the literature, e.g., by Gerritsen and Sabisky.[6] The program also takes into account the Boltzmann population factor in calculating the transition intensities.

The starting point for simulations of MnTPPCl spectra was the previously obtained set of spin-Hamiltonian parameters ($D = -2.27$ cm^{-1}, $E = 0$, and $g = 1.82$).[21] This parameter set produced an immediate good agreement between the simulation and experiment but was subsequently refined. In particular, $D = -2.290(5)$ cm^{-1} slightly improved the fit, which also gives a measure of the fit precision. In the previous study,[21] it was impossible to determine $g_{\perp}$ directly, but here the simulations allowed its determination as $g_{\perp} = 2.005(3)$. As for $g_{||}$, this was derived here again mainly from the single parallel transition, $|-2> \rightarrow |1>$ (the other parallel transition observable, $|-1> \rightarrow |0>$, being very weak). The accuracy of g determination depends linearly on resonance field, and the $|-2> \rightarrow |-1>$ transition appears at low field and is thus quite insensitive to variation in g. As a result, $g_{||}$ was obtained with poorer accuracy and was fixed at $g_{||} = 1.98(2)$. This value is much closer to g_e than the previously reported value (1.82) and is thus more reasonable, as will be shown below. The final set of parameters is presented in Table 1.

Comparison of the experimental and simulated spectra shows that agreement is nearly perfect with regard to the spectral position of the resonances and almost as good in the case of

line shape and intensities. The criterion for the "goodness of fit" was that neither of the observed resonance fields differs from the corresponding simulated peak by more than one-third of the line width. The minimal values of the simulated parameters which caused larger variations were used in calculating the error values presented in Table 1. Particularly nice is the appearance of the "twinned" perpendicular $|-1>\rightarrow|0>$ transition at both 280 and 374 GHz which was not predicted on the basis of the calculated plots discussed above. The extra peak corresponds to a turning point about 70° from the canonical position and could therefore not be calculated by the method of Baranowski et al.[29] The few small discrepancies between the simulation and experiment are the following: the three perpendicular transitions, each visible at 280 GHz and at 374 GHz, show a somewhat asymmetric shape which is not reproduced in simulations. In the case of the $|-1>\rightarrow|0>$ perpendicular transition one can even see a slight splitting of that transition. An obvious interpretation of this phenomenon would be a nonzero E value. However, any attempt at simulating the spectra with $|E|$ larger than 0.01 cm^{-1} results in a splitting primarily of the $|-2>\rightarrow|-1>$ perpendicular transition, which is not observed. It can thus be stated that the present result limits the magnitude of E to 0.01 cm^{-1} although even this value is probably conservative and the systems under study are rigorously axial. Another, more significant, discrepancy appears in the low-frequency (110 GHz) spectra as in Figure 2. One can see that the simulated intensity of the low-field (1 T) peak does not correspond to the experiment. This has most probably to do with the fact that this is a $\Delta M_S = \pm 2$ transition for which the program does not allow one to parametrize the line width. Another possible explanation of the dominance of the $|\Delta M_s| = 2$ transition in the experimental 110 GHz spectrum, namely some misalignment of B_1 field parallel to the B_0 can be ruled out since in spectra recorded at other frequencies, and also in spectra of other high-spin non-Kramers systems recorded in the same probe, notably Cr(II),[23] this problem did not appear. Altogether, the simulations confirmed the negative sign of D (with positive D the resonance fields are the same, but the intensities are very different).

Although the experimental HFEPR spectra of MnPcCl show a remarkable similarity to MnTPPCl, suggesting a very similar set of spin-Hamiltonian parameters, we first followed the procedure as outlined previously[21] and performed a multifrequency experiment (Figure 4). A linear fit of the resonance field vs frequency yields in a straightforward way the spin Hamiltonian parameters $D = -2.28$ cm^{-1} and $g = 2.02$. The nearly ideal straight slope of the frequency dependence of the $|-2>\rightarrow|-1>$ parallel resonance field means that the parameter E is zero, as discussed previously.[21] This set of parameters was the starting point for simulations, which refined the parameters to the following values: $D = -2.31(1)$ cm^{-1}, $E = 0$, and $g_{||} = 2.00(2)$ and $g_{\perp} = 2.005(5)$. The quality of MnPcCl spectra, generally poorer than those of MnTPPCl, is reflected in the error estimates.

Relation of EPR Parameters to Electronic Structure. For the first time, complete sets of accurate electronic parameters are available for two Mn(III) complexes of porphyrinic ligands. Previous studies have been performed using magnetic susceptibility[31,32] and far-IR spectroscopy,[33] which provided good measures of D but are relatively insensitive to E and to the g values. The parameters obtained here from HFEPR can be related to the electronic structure of these Mn(III) complexes, as was done qualitatively by Dugad et al.[32] using magnetic data. As given by Dugad et al.[32] following earlier work,[2,6] and similar to what we employed for aqueous Cr(II),[23] the following equations can be derived for an axial system with $S = 2$ and an electronic ground state with the "hole" in the $d_{x^2-y^2}$ orbital ($^5B_1$ ground state in the C_{4v} point group, appropriate for monoaxially coordinated metalloporphyrins):

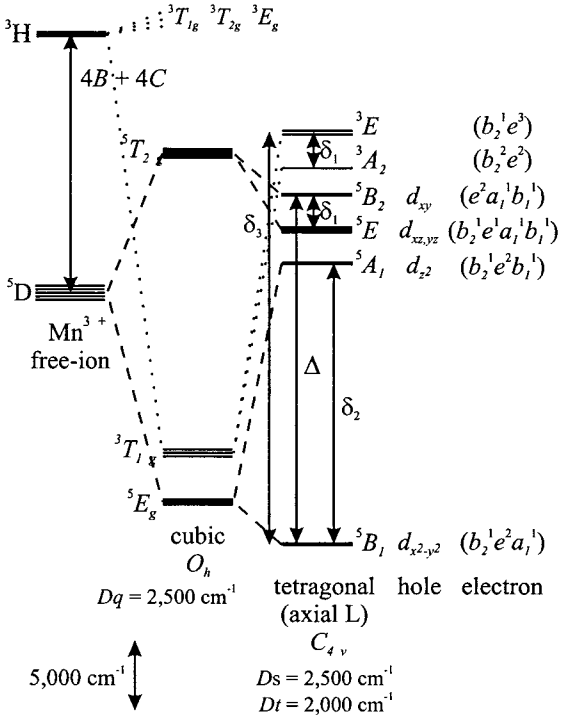

Figure 6. Energy level diagram for Mn(III) complexed by a porphyrinic ligand. The energies are based on calculations for CuPc[40] but rounded for easier relative scaling and clarity. The ligand field parameters are as defined by Ballhausen,[43] $Dq = 2500$ cm^{-1}, $Ds = 2500$ cm^{-1}, and $Dt = 2000$ cm^{-1}, and as defined by Dugad et al.,[32] $\Delta = 25\,000$ cm^{-1} ($=10Dq$), $\delta_1 = 2500$ cm^{-1} ($=-3Ds + 5Dt$), and $\delta_2 = 23\,100$ cm^{-1} ($=4Ds + 5Dt$). The energy of excited triplet state terms are also indicated. For ^3E, this is defined by δ_3, where $\delta_3 = [\Delta E(^3T_{1g} - {}^5E_g) + \delta_1 + \delta_2]$, where $\Delta E(^3T_{1g} - {}^5E_g)$ is determined by exact calculation; see text.

$$D = \lambda^2\{-4/\Delta + 1/(\Delta - \delta_1)\} + D' \quad (2a)$$

$$D' = \lambda^2(-4/\delta_3) \quad (2b)$$

$$g_{||} = g_e - 8\lambda/\Delta \quad (2c)$$

$$g_{\perp} = g_e - 2\lambda/(\Delta - \delta_1) \quad (2d)$$

Here λ is the spin−orbit coupling constant (88 cm^{-1} for free Mn^{3+}). The other parameters are electronic energy splittings as follows: Δ ($10Dq$) is the splitting between the $^5B_1$ ground state ($b_2^1e^2a_1^1$ electronic configuration) and the $^5B_2$ excited state ($e^2a_1^1b_1^1$ electronic configuration); $\Delta - \delta_1$ is the splitting between the $^5B_1$ ground state and the ^5E excited state ($b_2^1e^1a_1^1b_1^1$ electronic configuration); δ_3 is the splitting between the $^5B_1$ ground state and the ^3E excited state ($b_2^1e^3$ electronic configuration). A semiquantitative diagram depicting these energy levels is shown in Figure 6. The last of these parameters, δ_3, is more difficult to quantify since it involves an excited spin state ($S = 1$, as opposed to 2). In the strong-field approximation, appropriate for these porphyrinic systems, the lowest energy

(31) Behere, D. V.; Mitra, S. *Inorg. Chem.* **1980**, *19*, 992−995.
(32) Dugad, L. B.; Behere, D. V.; Marathe, V. R.; Mitra, S. *Chem. Phys. Lett.* **1984**, *104*, 353−356.
(33) Brackett, G. C.; Richard, P. L.; Caughey, W. S. *J. Chem. Phys.* **1971**, *54*, 4383−4401.

triplet excited state is $^3T_{1g}$ (t_{2g}^4 electronic configuration) in cubic (O_h) symmetry.[34,35] This $^3T_{1g}$ state in a strong-field arises from a number of free-ion terms (^{3}G, ^{3}H(2), ^{3}F(2), ^{3}P(2)) but primarily from ^{3}H. In a strong-field, if only diagonal elements are considered, which is commonly done for convenience,[32] then the energy splitting is $\Delta E(^3T_{1g} - {}^5E_g) = \{(-15B + 5C - 16Dq) - (-21B - 6Dq)\} = 6B + 5C - \Delta$, where B and C are the Racah parameters.[34,35] We determined $\Delta E(^3T_{1g} - {}^5E_g)$ exactly by diagonalization of the 7 × 7 matrix given by McClure,[35] which includes all the free-ion contributions. This $^3T_{1g}$ state is in turn split into ^{3}E and $^3A_2$ states in axial (C_{4v}) symmetry (see Figure 6). The energies of the ^{3}E and $^3A_2$ states are then given to first-order as $E(^3E) = \delta_3 = [\Delta E(^3T_{1g} - {}^5E_g) + \delta_1 + \delta_2]$ and $E(^3A_2) = [\Delta E(^3T_{1g} - {}^5E_g) + \delta_2]$.[32] The significance of the triplet state energies will be discussed below. The contribution of this excited state to the zfs (i.e. the derivation of eq 2b) is given in the Appendix.

Electronic Structure for Metalloporphyrinic Complexes. In many transition metal complexes, the energy levels are accurately known from electronic absorption spectroscopy and EPR parameters can be directly calculated for comparison with experiment. This type of quantitative analysis was performed in our study of aqueous Cr(II)[23] and by Barra et al. in their HFEPR study of Mn(dbm)$_3$.[22] Unfortunately, in the case of metalloporphyrinic complexes, this type of analysis is not possible. The electronic absorption spectra are totally dominated by transitions involving the π-conjugated macrocyclic ligand, overwhelming the relatively weak d−d transitions.[36−38] For example, the electronic absorption spectrum of MnPc(OAc) in DMF solution has been very carefully studied by Lever at al.,[36] and although numerous bands were assigned to ligand-to-ligand transitions, ligand-to-metal, and metal-to-ligand charge-transfer transitions, none was definitively assigned to a d−d transition. Lever et al. speculated that a transition at 10 670 cm^{-1} might be d−d in origin but ruled out this assignment because the same transition was observed for the Cr(III) analogue.[36]

Another source of electronic energy levels is from theoretical calculations. Again, there are unfortunately no studies directly relevant to these Mn(III) complexes. Extended Hückel calculations have been made by Schaffer et al.[39] for phthalocyanine complexes of several M(II) ions (M = Mn, Fe, Co, Ni), which showed a relatively narrow range of 10Dq values: 22 000−27 000 cm^{-1}, based on visual inspection of their figures. Of much greater relevance is a semiempirical MO calculation that was done on CuPc by Henriksson et al.,[40] which explicitly considers the metal ion 3d, 4s, and 4p orbital energies. The calculations obtained by this method for CuPc were in good agreement with EPR data.[41,42] This complex is a reasonable analogue to the systems studied here since Cu(II) can be thought of as a d^{10} system with a "hole", just as HS Mn(III) is a d^5 system with a "hole". Thus CuPc has a $^5B_{1g}$ ground state (D_{4h} point group for this square planar complex) and an energy level diagram much like that in Figure 6. Henriksson et al. calculated d−d transition energies for CuPc.[40] Their results allow determination of Cu(II) 3d orbital energy levels using the ligand field parameters conveniently described by Ballhausen:[43] $Dq = 2680$ cm^{-1}, $Ds = 2800$ cm^{-1}, and $Dt = 2380$ cm^{-1}, where $10Dq = \Delta = 26\,800$ cm^{-1}, $-3Ds + 5Dt = \delta_1 = 3500$ cm^{-1}, and $4Ds + 5Dt = \delta_2 = 23\,100$ cm^{-1}.

With this CuPc model as a starting point, we can use eqs 2 to make semiquantitative comparisons between experimental and calculated EPR parameters. If we initially neglect the excited triplet state contribution ($D' \equiv 0$), then eq 2a with the free-ion λ value gives $D \approx -0.82$ cm^{-1} and eqs 2c,d give $g_{||} \approx 1.976$ and $g_\perp \approx 1.995$. This is quite reasonable for the g values obtained accurately here but much too small in magnitude for D (see Table 1). Using the experimental $D = -2.31$ cm^{-1}, then eq 2b suggests that the balance, contributed by the triplet excited state, is $D' = -1.49$ cm^{-1}, so that $\delta_3 \approx 20\,800$ cm^{-1}. This value can then be compared to that obtained from the Racah parameters and ligand field terms. As we have done previously,[23] two sources of free-ion values for Mn^{3+} are used: $B = 965$ cm^{-1}, $C = 4450$ cm^{-1};[35] $B = 1140$ cm^{-1}, $C = 3650$ cm^{-1}.[44] Using the exact calculation, with this large cubic field and either set of Racah parameters, the $^3T_{1g}$ state is actually lower in energy than the ^5E_g state by ca. 400 or 3400 cm^{-1} using the Racah parameters taken from McClure[35] or from Mabbs and Collison,[44] respectively. Inclusion of the large axial term, here simply to first-order as done by Dugad et al.,[32] gives $\delta_3 \approx 26\,200$ or 23 200 cm^{-1}, respectively as above. The latter of these values gives $D' = -1.34$ cm^{-1}, so that a calculated $D \approx -2.16$ cm^{-1}. Given the massive assumption made here, namely the direct application of theoretical parameters for CuPc (albeit supported by its EPR data[41,42]) to MnPcCl, this agreement between experimental and calculated zfs parameters is remarkable. Qualitatively, it is likely that both Δ and δ_2 are smaller in MnPcCl than in CuPc, but their relative changes are impossible to determine without sophisticated theoretical studies. It is similarly likely that both λ and B are reduced from their free-ion values. These effects have been quantified for homoleptic octahedral complexes lacking Jahn−Teller distortion (e.g., d^3 and HS d^5 species such as $[Mn(H_2O)_6]^{2+}$),[45] but the porphyrinic Mn(III) complexes studied here cannot be easily categorized this way. A decrease in λ would shift the g values even closer to g_e, as observed, but decrease the magnitude of D; however a corresponding decrease in B would decrease δ_3 thus increasing the magnitude of D'. Again, it is impossible here to quantify these counteracting effects.

Comparison of Fit Parameters Among Related Complexes. As can be seen from Table 1, Mn(III) porphyrinic complexes are quite similar but are distinctly different from pseudooctahedral complexes that have been studied by EPR. The former have much smaller magnitude zfs and are rigorously axial systems. These are likely the consequences of the geometry imposed by the square planar, more strongly covalent bonding porphyrinic ligand. Although monoaxially coordinated Mn(III) porphyrinic complexes are high-spin ($S = 2$), the analysis of HFEPR data for MnPcCl and MnTPPCl suggests that triplet excited states are relatively low-lying in energy. This spin-state

(34) Griffith, J. S. *The Theory of Transition-Metal Ions*; Cambridge University Press: Cambridge, U.K.; 1964; Chapter 4.
(35) McClure, D. S. *Solid State Phys.* **1959**, *9*, 399−525.
(36) Lever, A. B. P.; Pickens, S. R.; Minor, P. C.; Licoccia, S.; Ramaswamy, B. S.; Magnell, K. *J. Am. Chem. Soc.* **1981**, *103*, 6800−6806.
(37) Stillman, M. J.; Nyokong, T. In *Phthalocyanines: Properties and Applications*; Leznoff, C. C., Lever, A. B. P., Eds.; VCH Publishers: New York, 1989; Vol. 1, pp 133−289.
(38) Gouterman, M. In *The Porphyrins*; Dolphin, D., Ed.; Academic Press: New York, 1978; Vol. III, Part A., Physical Chemistry, pp 1−165.
(39) Schaffer, A. M.; Gouterman, M.; Davidson, E. R. *Theor. Chim. Acta* **1973**, *30*, 9−30.
(40) Henriksson, A.; Roos, B.; Sundbom, M. *Theor. Chim. Acta* **1972**, *27*, 303−313.
(41) Chen, I.; Abkowitz, M.; Sharp, H. *J. Chem. Phys.* **1969**, *50*, 2237−2244.
(42) Guzy, C. M.; Raynor, J. B.; Symons, M. C. R. *J. Chem. Soc. (A)* **1969**, 2299−2303.
(43) Ballhausen, C. J. *Introduction to Ligand Field Theory*; McGraw-Hill: New York, 1962; pp 99−103.
(44) Mabbs, F. E.; Collison, D. *Electron Paramagnetic Resonance of d Transition Metal Compounds*; Elsevier: Amsterdam, 1992; p 322.
(45) Jorgensen, C. K. *Discuss. Faraday Soc.* **1958**, *26*, 110−115.

ambiguity is supported by the ground states observed for related metalloporphyrinic complexes. For example, MnPc,[46] FePc,[46] and FeTPP,[47] all of which have no axial coordination, have ground states with intermediate spin, $S = {}^3/_2$ for d^5 Mn(II) and $S = 1$ for d^4 Fe(II), and with bis-axial coordination, low-spin ground states are observed. $MnPc(Et_3N)_2$[48] has $S = {}^1/_2$ and $FeTPP(pip)_2$[47] has $S = 0$. As suggested by these results, and as seen in our previous study[21] and by others,[32−34,48] the effect of axial ligation on the electronic parameters of Mn(III) is quite noticeable. The magnitude of D increases as the axial coordination strengthens, e.g., six-coordinate MnTPP(py)Cl has the largest magnitude D and MnTPPBr the smallest (see Table 1). Stronger axial coordination decreases δ_1 increasing the magnitude of D as given by eqs 2a,b. This effect should also be manifest in the g values (eqs 2c,d); however, the magnetic measurements are insufficiently sensitive to detect this effect. Further HFEPR studies on other integer spin porphyrinic complexes will shed light on these electronic effects. It is also hoped that experimental data obtained from HFEPR will inspire further, complementary theoretical work.

Conclusions

HFEPR spectroscopy allows the observation of EPR spectra from transition metal complexes traditionally considered as "EPR-silent", such as axially symmetric Mn(III) in MnTPPCl and MnPcCl, studied here. One difficulty, however, with HFEPR is that the high fields can lead to orientation of powder samples with respect to the external magnetic field. This orientation precludes observation of the powder pattern spectra necessary to obtain a complete parametrization of the metal ion. We have shown that immobilization of powder either by preparation of either *n*-eicosane mulls or KBr pellets, the former method borrowed from magnetization studies and the latter from IR spectroscopy, leads to ideal powder pattern HFEPR spectra that can be well simulated. The parameters obtained from this analysis of MnTPPCl and MnPcCl HFEPR spectra provide estimates of electronic energy levels. The resulting energy diagram shows the significant involvement of a triplet excited state, which is in agreement with the observation of lower spin states in other metalloporphyrinic complexes. This information is essentially impossible to obtain directly from electronic absorption spectroscopy because the extremely strong ligand-based transitions obscure any d−d transitions. Comparison among Mn(III) porphyrinic complexes shows the effect of axial ligation wherein the stronger axial coordination is manifest in larger magnitude zfs.

Appendix: Contribution of a Triplet Excited State to the Zero-Field Splitting of the Quintet Ground State in HS d^4

1. Energy Separation. In the free ion, only excited-state terms that differ from the ground state by $\Delta L = 0, \pm 1$ and $\Delta S = 0, \pm 1$ (and $\Delta J = 0$) are allowed to interact via spin−orbit coupling to the ground state.[34] In the HS d^4 system of interest here, the free-ion term from which the quintet ground-state originates is ^{5}D (at an energy $-21B$). As there are no other quintet states, only triplet excited states may interact, and of these, only ^3P_a (at an energy $-5B + 5.5C - 0.5(912B^2 - 24BC + 9C^2)^{1/2}$) is allowed ($\Delta L = -1$). The free-ion term ^{3}H is closer in energy (at an energy $-17B + 4C$) for typical Racah parameters but corresponds to $\Delta L = 3$. The system of interest, however, is best represented by a strong-field model, in which case the free ion terms are no longer pure states but are mixed. As a result, the relevant representation in a cubic field for the ground state is ^5E_g (t_2^3e) and that for nearest triplet excited state is $^3T_{1g}$ (t_2^4), which involves contributions from six free-ion terms: ^{3}H (contributing twice), $^3P_{a,b}$, $^3F_{a,b}$, and ^{3}G.[34,35] If the off-diagonal electron−electron repulsion terms are ignored, then, in a cubic strong-field, the energy separation between the ground quintet and lowest triplet state is $\Delta E(^3T_{1g} - {}^5E_g) = [(-15B + 5C - 16Dq) - (-21B - 6Dq)] = [6B + 5C - 10Dq] = [6B + 5C - \Delta]$. In a tetragonal field (C_{4v} symmetry), relevant to the axially coordinated Mn(III) porphyrinic complexes studied here, the ground state is $^5B_1$, as shown in Figure 6, and the relevant excited state is ^{3}E. As given by Dugad et al.,[32] the energy splitting of the ^{3}E state is $\delta_3 = [\Delta E(^3E - {}^5B_1)] \approx [\Delta E(^3T_{1g} - {}^5E_g) + \delta_1 + \delta_2] \approx [6B + 5C - \Delta + \delta_1 + \delta_2]$. For improved accuracy, we determined $\Delta E(^3T_{1g} - {}^5E_g)$ exactly by diagonalization of the 7×7 matrix given by McClure[35] and Griffith[34] and then included estimates for δ_1 and δ_2 to give the net energy splitting, $\delta_3 = \Delta E(^3E - {}^5B_1)$, as described in the text.

2. Spin−Orbit Contribution. Given this energy splitting, then next matter is to determine the contribution via spin−orbit coupling of the ^{3}E excited state to the $^5B_1$ ground state. The easiest way to accomplish this is to represent these states by Slater type determinants,[43] as used extensively, for example, by McGarvey.[49] In this system, the ground spin−orbital states are as follows:

$$^5B_1(M_S = 2) = d_{xy}^{+}d_{xz}^{+}d_{yz}^{+}d_{z^2}^{+}$$

$$^5B_1(M_S = 1) = (1/2)(d_{xy}^{+}d_{xz}^{+}d_{yz}^{+}d_{z^2}^{-} + d_{xy}^{+}d_{xz}^{+}d_{yz}^{-}d_{z^2}^{+} + d_{xy}^{+}d_{xz}^{-}d_{yz}^{+}d_{z^2}^{+} + d_{xy}^{-}d_{xz}^{+}d_{yz}^{+}d_{z^2}^{+})$$

$$^5B_1(M_S = 0) = (1/6)^{1/2}(d_{xy}^{+}d_{xz}^{+}d_{yz}^{-}d_{z^2}^{-} + d_{xy}^{+}d_{xz}^{-}d_{yz}^{-}d_{z^2}^{+} + d_{xy}^{+}d_{xz}^{-}d_{yz}^{+}d_{z^2}^{-} + d_{xy}^{-}d_{xz}^{-}d_{yz}^{+}d_{z^2}^{+} + d_{xy}^{-}d_{xz}^{+}d_{yz}^{+}d_{z^2}^{-} + d_{xy}^{-}d_{xz}^{+}d_{yz}^{-}d_{z^2}^{+})$$

Here the plus and minus superscripts refer to the spin quantization and the determinants are ordered by following the MO scheme of Dugad et al.[32] Any interchange in the order of two d orbitals produces a change in sign of the function. The corresponding functions for the $^3E(M_S)$ state can be written as

$$^3E_a(M_S = 1) = d_{xy}^{+}d_{xz}^{+}d_{xz}^{-}d_{yz}^{+}$$

$$^3E_a(M_S = 0) = (1/2)^{1/2}(d_{xy}^{+}d_{xz}^{+}d_{xz}^{-}d_{yz}^{-} + d_{xy}^{-}d_{xz}^{+}d_{xz}^{-}d_{yz}^{+})$$

$$^3E_b(M_S = 1) = d_{xy}^{+}d_{xz}^{+}d_{yz}^{+}d_{yz}^{-}$$

$$^3E_b(M_S = 0) = (1/2)^{1/2}(d_{xy}^{+}d_{xz}^{-}d_{yz}^{+}d_{yz}^{-} + d_{xy}^{-}d_{xz}^{+}d_{yz}^{+}d_{yz}^{-})$$

What is needed are the matrix elements between the two states for the spin−orbit operator, $\mathbf{H}_{LS}$:

$$\mathbf{H}_{LS} = \xi\sum_i l_{zi}s_{zi} + l_{xi}s_{xi} + l_{yi}s_{yi}$$

Here ξ is the single-electron spin−orbit coupling constant. Using the relationships

(46) Kirner, J. F.; Dow, W.; Scheidt, W. R. *Inorg. Chem.* **1976**, *15*, 1685.
(47) Collman, J. P.; Hoard, J. L.; Kim, N.; Lang, G.; Reed, C. A. *J. Am. Chem. Soc.* **1975**, *97*, 2676−2681.
(48) Lever, A. B. P.; Quan, S. K. *Inorg. Chem.* **1981**, *20*, 761−768.
(49) McGarvey, B. R. *Inorg. Chem.* **1995**, *34*, 6000−6007.

$$l_z d_{xy} = -2i d_{x^2-y^2} \quad l_x d_{xy} = i d_{xz} \quad l_y d_{xy} = -i d_{yz}$$

$$l_z d_{xz} = i d_{yz} \quad l_x d_{xz} = -i d_{xy} \quad l_y d_{xz} = 3^{1/2} - i d_{z^2} + i d_{x^2-y^2}$$

$$l_z d_{yz} = -i d_{xz} \quad l_x d_{yz} = 3^{1/2} i d_{z^2} + i d_{x^2-y^2} \quad l_y d_{yz} = i d_{xy}$$

it can be seen that, in this case, only l_x and l_y respectively couple the ^3E_b and ^3E_a states to $^5B_1$, since only these can generate d_{z^2}. Thus $\mathbf{H}_{LS}$ operating on each of the ^3E states gives the following:

$$\mathbf{H}_{LS}|^3E_a(0)> = \xi(3/8)^{1/2}\{d_{xy}^{+}d_{xz}^{+}d_{yz}^{-}d_{z^2}^{+} + d_{xy}^{-}d_{xz}^{+}d_{yz}^{+}d_{z^2}^{+} + d_{xy}^{+}d_{xz}^{-}d_{yz}^{-}d_{z2}^{-} + d_{xy}^{-}d_{xz}^{-}d_{yz}^{+}d_{z^2}^{-}\}$$

$$\mathbf{H}_{LS}|^3E_a(1)> = \xi(3/4)^{1/2}\{d_{xy}^{+}d_{xz}^{+}d_{yz}^{+}d_{z^2}^{+} + d_{xy}^{+}d_{xz}^{-}d_{yz}^{+}d_{z^2}^{-}\}$$

$$\mathbf{H}_{LS}|^3E_b(0)> = \xi(3/8)^{1/2}i\{d_{xy}^{+}d_{xz}^{-}d_{yz}^{+}d_{z^2}^{+} + d_{xy}^{-}d_{xz}^{+}d_{yz}^{+}d_{z^2}^{+} - d_{xy}^{+}d_{xz}^{-}d_{yz}^{-}d_{z^2}^{-} - d_{xy}^{-}d_{xz}^{+}d_{yz}^{-}d_{z^2}^{-}\}$$

$$\mathbf{H}_{LS}|^3E_b(1)> = \xi(3/4)^{1/2}i\{d_{xy}^{+}d_{xz}^{+}d_{yz}^{+}d_{z^2}^{+} - d_{xy}^{+}d_{xz}^{+}d_{yz}^{-}d_{z^2}^{-}\}$$

Here all the terms that do not belong to $^5B_1$ (i.e., those with $d_{x^2-y^2}$) have been dropped. This gives the following nonzero matrix elements:

$$<^5B_1(2)|\mathbf{H}_{LS}|^3E_a(1)> = (3/4)^{1/2}\xi \qquad <^5B_1(2)|\mathbf{H}_{LS}|^3E_b(1)> = (3/4)^{1/2}i\xi$$

$$<^5B_1(1)|\mathbf{H}_{LS}|^3E_a(0)> = (3/8)^{1/2}\xi \qquad <^5B_1(1)|\mathbf{H}_{LS}|^3E_b(0)> = (3/8)^{1/2}i\xi$$

$$<^5B_1(0)|\mathbf{H}_{LS}|^3E_a(1)> = (1/8)^{1/2}\xi \qquad <^5B_1(0)|\mathbf{H}_{LS}|^3E_b(1)> = (1/8)^{1/2} - i\xi$$

Using these matrix elements, second-order perturbation theory allows us to calculate the contribution of ^3E to $^5B_1(M_S)$, which is

$$\Delta E'(2) = -(3/2)\xi^2/[\Delta E(^3E - {}^5B_1)]$$

$$\Delta E'(1) = -(3/4)\xi^2/[\Delta E(^3E - {}^5B_1)]$$

$$\Delta E'(0) = -(1/2)\xi^2/[\Delta E(^3E - {}^5B_1)]$$

For the $S = 2$ system $\{E(M_S = \pm 2) - E(M_S = \pm 1)\} = 3D$ and $\{E(M_S = \pm 1) - E(M_S = 0)\} = D$, therefore

$$D' = -(1/4)\xi^2/[\Delta E(^3E - {}^5B_1)]$$

which corresponds to eq 2b, using $\xi = 2S\,\lambda = 4\lambda$.

If the ground state were $^5A_1$, then the above procedure gives the value

$$D' = -(1/12)\xi^2/[\Delta E(^3E - {}^5A_1)]$$

since the factor $3^{1/2}$ is absent from the $\mathbf{H}_{LS}$ operations.

Acknowledgment. This work was supported by the NHMFL (J.K., L.A.P., and L.-C.B.). J.T. was supported by Roosevelt University and the NHMFL User Program. We thank Dr. H. Weihe from the University of Copenhagen, Copenhagen, Denmark, for providing us with the EPR simulation program, as well as explaining its details, and Dr. M. J. Knapp from UC—Berkeley for suggesting the *n*-eicosane method of immobilizing the sample. We also very gratefully acknowledge Prof. B. R. McGarvey, University of Windsor, Canada, for deriving the material presented in the Appendix.

IC9901970